Journal of Alloys and Compounds 509 (2011) 2914–2918

Contents lists available at ScienceDirect

Journal of Alloys and Compounds

journal homepage: www.elsevier.com/locate/jallcom

Room temperature ferromagnetism and magnetoelectric coupling in $(K_{0.5}Na_{0.5})NbO_3$ PLD nanocrystalline films

Ensi Cao, Jifan Hu*, Hongwei Qin, Feng Ji, Minglei Zhao, Minhua Jiang

Department of Physics, State Key Laboratory for Crystal Materials, Shandong University, Jinan 250100, People's Republic of China

ARTICLE INFO

Article history:
Received 2 September 2010
Received in revised form
19 November 2010
Accepted 22 November 2010
Available online 30 November 2010

Keywords:
Room-temperature ferromagnetism
Cation vacancy
Magnetoelectric coupling
PLD film
Multiferroics

ABSTRACT

$(K_{0.5}Na_{0.5})NbO_3$ nanocrystalline films have been successfully prepared on conductive Si substrate under different conditions by pulsed laser deposition. Room temperature ferromagnetism has been achieved through the introduction of cation (K, Na) vacancies during deposition at the expense of the deterioration of ferroelectricity. In addition to positive magnetocapacitance effect and electrical manipulation of magnetization, the new phenomenon that the orthometric application of an electric field and magnetic field on the surface of film leads to an enormous enhancement of in-plane saturation magnetization has been first observed, indicative of a strong magnetoelectric coupling which has a memory effect on the saturation magnetization at room temperature.

1. Introduction

In recent years, multiferroic materials exhibiting coexistence and simultaneous coupling of ferroelectricity and ferromangtism/antiferromagntism have received considerable attention due to their fascinating physical properties and potential applications [1–5]. Most of recent researches on single-phase multiferroic materials are concentrated on the modified $BiFeO_3$ (BFO) ceramics and films. Various A-site or B-site substitutions by rare-earth ions have been used to modify the multiferroic properties [6–14]. However, BFO is known to be ferroelectric and antiferromagntic at room temperature, multiferroic material which shows room temperature ferromagnetism (RTFM) is still rare.

RTFM has already been observed in undoped oxides such as HfO_2, TiO_2, ZnO, SnO_2, In_2O_3, Al_2O_3 and MgO in forms of nanograins or films [15–22]. Some experimental results indicated that the unexpected ferromagnetism in HfO_2 and TiO_2 originated from oxygen vacancies [16,22], however, an ab initio calculation suggested that it was Hf vacancies that bring about the ferromagntism for HfO_2 [23]. For MgO, both experimental and theoretical results demonstrated that ferromagnetism originated from the Mg vacancies [19–21,24,25].

In order to obtain room temperature single phase multiferroic material, an alternative way is to introduce RTFM into room temperature ferroelectric oxide materials through intrinsic defects, such as cation or oxygen vacancies. Room temperature multiferroic behaviors with magnetocapacitance (MC) or magnetodielectric (MD) effect has been observed in undoped $BaTiO_3$ and $La_2Ti_2O_7$ nanocrystalline pellets [26,27], but have not been reported in ferroelectric materials in the form of films, while most of the pulsed laser deposited oxide films showed weak RTFM.

$(K_{0.5}Na_{0.5})NbO_3$ (KNN) is a promising lead-free piezoelectric material, with a high Curie temperature, good ferroelectric and piezoelectric properties as well as biocompatibility [28]. Most of the recent researches are focused on the modified KNN ceramics to improve their electrical properties [29–35]. In addition, many preparation techniques such as magnetron sputtering [36,37], pulsed laser deposition (PLD) [38,39], metal-organic chemical vapor deposition (MOCVD) [40], sol–gel methods [41,42] and chemical solution approach [43], have been employed to obtain KNN thin films with high quality. However, it is difficult to control the stoichiometric composition of the resulting KNN thin films due to the strong volatilization of K and Na during PLD, which, on the other side, can also be utilized to investigate the influence of cation vacancies on the magnetic properties of KNN films. Here we first report that RTFM can be achieved in pulsed laser deposited KNN nanocrystalline films through the introduction of intrinsic defects during deposition, and the magnetoelectric coupling was demonstrated by the magnetcocapacitance effect and the enhancement of saturation magnetization after electric field treatment.

2. Experimental

The ceramic target of KNN was prepared using highly purified raw materials (99.99%) by the conventional solid-state sintering process. Ablation of the target

* Corresponding author. Tel.: +86 531 88377035; fax: +86 531 88377031.
E-mail address: hu-jf@vip.163.com (J. Hu).

0925-8388/$ – see front matter © 2010 Elsevier B.V. All rights reserved.
doi:10.1016/j.jallcom.2010.11.155

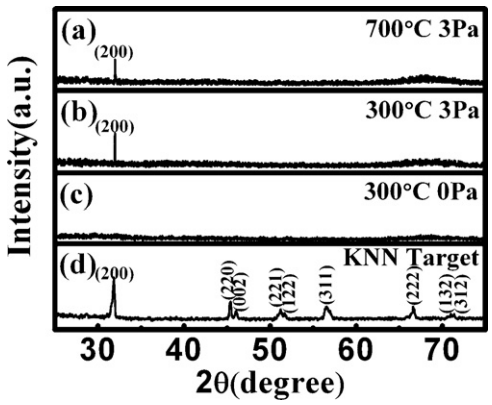

Fig. 1. XRD patterns for KNN film deposited under different conditions (a): T_s = 700 °C, P_{O_2} = 3 Pa; (b): T_s = 300 °C, P_{O_2} = 3 Pa; (c): T_s = 300 °C, P_{O_2} = 0 Pa; (d): KNN target.

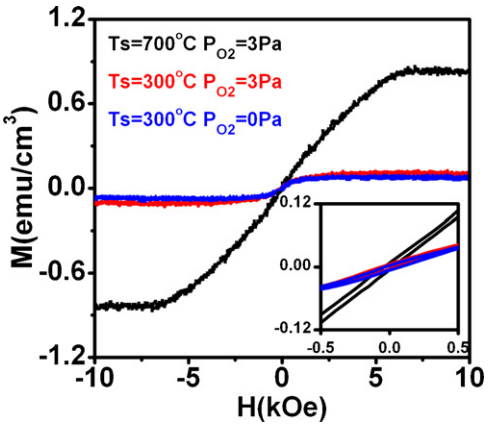

Fig. 2. Field dependence of magnetization for KNN films with different deposition conditions. The inset represents the field dependence of magnetization in the low field range.

was achieved using a KrF excimer laser source (λ = 248 nm, pulse duration of 20 ns, repetition rate of 5 Hz). The KNN nanocrystalline films were directly deposited on conductive Si substrate (ρ = 0.02 Ω cm) at substrate temperature (T_s) ranging from 300 °C to 700 °C, under oxygen pressure (P_{O_2}) in the range of 0–3 Pa. All substrates were ultrasonically cleaned in acetone, ethanol and deionized water sequently, followed by dipping into 10 wt% HF solution for 5 min to remove the surface oxide layer. The cleaned substrates were loaded into the processing chamber immediately to minimize possible formation of native oxide. The substrate temperature (T_s) was increased to the set value in a high vacuum atmosphere of 2×10^{-5} Pa to avoid the formation of silicon oxide during the heating process, then the T_s and incident laser energy were kept at the set value and 150 mJ/pulse, respectively, during deposition. The distance between the substrate and the target was kept at 80 mm and the deposition duration was 2 h for all the depositions. All the as-deposited films were post-annealed at 800 °C for 1 h in air. The film thickness was determined with a profilometer. Magnetic properties of the samples were measured using an alternating gradient magnetometer (AGM, Model: MicroMag 2900 from the Princeton Measurements Corporation, USA), which has an extremely high sensitivity of 10 nemu at room temperature, with magnetic field parallel to the surface of the KNN film. Ferroelectric properties of the sample were examined by measuring the polarizations (P) against the electric field (E) loop at room temperature by a ferroelectric meter (Radiant Premier II).

3. Results and discussion

Fig. 1 shows the X-ray diffraction patterns (with Cu Kα radiation) for the KNN films deposited under different conditions: (a) T_s = 700 °C, P_{O_2} = 3 Pa; (b) T_s = 300 °C, P_{O_2} = 3 Pa; (c) T_s = 300 °C, P_{O_2} = 0 Pa and (d) KNN target. For convenience of discussion below, the above films are labeled as Sample A (1.4 μm), Sample B (2 μm), and Sample C (2.4 μm), respectively. The target is polycrystalline in the orthorhombic phase with lattice parameters a = 5.6164 Å, b = 5.6999 Å, and c = 3.9397 Å, which are calculated from peak locations and Miller indices in the XRD patterns. The Si substrate adopted is (1 0 0) oriented, and the cubic lattice parameters are $a = b = c$ = 5.430 Å. The in-plane lattice mismatch between the KNN target and the Si substrate is so small that makes Si substrate suitable for the deposition of the KNN film. XRD patterns show textured KNN in the orthorhombic phase along (2 0 0) for Samples A and B, while no obvious peaks are visible in Sample C, indicating that oxygen atmosphere is prerequisite for the growth of KNN films, without which the deposited KNN film would be in amorphous state as Sample C. Therefore, we focused our work below mainly on the magnetic and ferroelectric properties of Sample A and Sample B. By comparing the XRD patterns for Sample A and Sample B, we found that with the increase of deposition temperature from 300 °C to 700 °C, the in-plane lattice parameter a decreased from 5.5948 Å to 5.5904 Å, both smaller than that of the target duo the compressive force form the substrate. The microstructure of the KNN films was examined by a field emission scanning electron microscope (FE-SEM). The average grain size of Sample B was about 100 nm, while larger grains in the average size of 300 nm appeared in the FE-SEM image of Sample A, because higher substrate temperature faciliated the growth of nanocrystals.

The field dependence of magnetization for the KNN films after correction of diamagnetic signal of the Si substrate and measuring probe is displayed in Fig. 2. Clear hysteresis loops can be observed (see the inset of Fig. 2), showing the existence of FM. As all the measurements were carefully performed to avoid possible contaminations from environment, sample handling or measurement procedure [44], and no diffraction peaks from impurity phase can be observed in the XRD patterns, the observed FM should be intrinsic property of the KNN film, rather than extrinsic effect. The saturation magnetization (M_s) of Sample B is just 0.11 emu/cm^3. To explore the possible origin of FM in the KNN film, we also deposited one sample at T_s = 300 °C in vacuum and another sample at T_s = 700 °C under P_{O_2} = 3 Pa, with other preparation conditions same for all. The M_s of Sample C is 0.073 emu/cm^3, slightly smaller than that of Sample B. Since the deposition in vacuum usually introduces more oxygen vacancies into semiconductors or insulator oxides, the observed FM should be less associated with oxygen vacancies. On the other hand, the M_s of Sample A is 0.83 emu/cm^3, much larger than that of Sample B. High substrate temperature deposition usually increases the vaporization of alkali elements, which results in the increase of cation vacancies in the deposited film [45]. Therefore, the observed RTFM in the KNN nanocrystalline films is more associated with the cation (K, Na) vacancies, rather than oxygen vacancies.

The capacitor structure of Si/ED/FE/ED is usually adopted in the deposition of ferroelectric films on Si substrate by PLD, where FE represents ferroelectric thin film, and ED denotes conductive metallic oxide buffer layer (such as $SrRuO_3$ [46], $LaNiO_3$ [47]) or metallic electrode material (such as Pt, Pd). However, the buffer layer electrodes might have certain influence on the magnetic signal of the sample and make the problem complicated. Therefore we deposited KNN films directly on Si substrate, and deposited Pt electrodes in the square of 1 mm × 1 mm onto the center of both sides of the sample by evaporation to take the ferroelectric measurement.

As shown in Fig. 3, unsaturated P–E hysteresis loops were observed. Although the observed PE loops are similar to those reported for bananas [48], the KNN film prepared in this work crystallizes in the orthorhombic phase, which has been found to be a ferroelectric phase for KNN materials [49]. The PE loops shown here demonstrate that RTFM can be achieved in conventional ferroelectric materials, such as KNN, through the introduction of cation vacancies during deposition at the expense of the deterioration of ferroelectricity. That is to say, the cation vacancies lead to the increase of leakage current, and result in unsaturated PE loops [50].

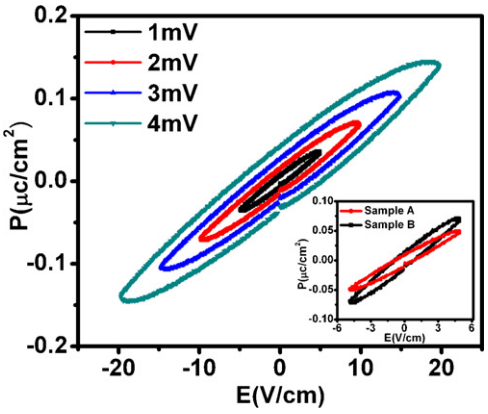

Fig. 3. Polarization versus electric field curves for Sample B (T_s = 300 °C, P_{O_2} = 3 Pa). The inset shows the *PE* loops for Sample A (T_s = 700 °C, P_{O_2} = 3 Pa) and Sample B under 1 mV.

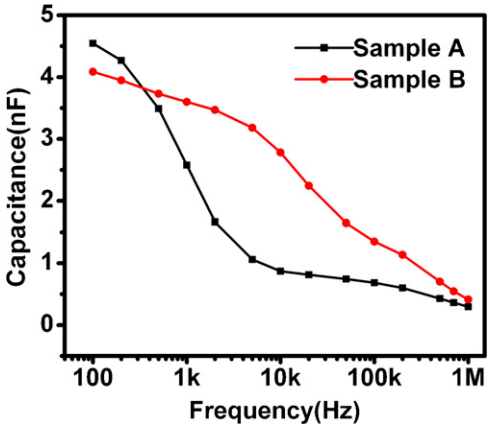

Fig. 4. Capacitance as a function of frequency for Sample A (T_s = 700 °C, P_{O_2} = 3 Pa) and Sample B (T_s = 300 °C, P_{O_2} = 3 Pa) at room temperature with zero magnetic field.

The inset shows the *PE* loops for Sample A and Sample B when 1 mV was applied to both samples. Because of the different film thicknesses, the electric field applied to Sample A is normalized to 5 V/cm for convenience of comparison. It can be seen that the electric polarization in sample A is slightly smaller than that in Sample B, meaning that with the increase of substrate temperature from 300 °C to 700 °C, the higher concentration of cation vacancies leads to the decrease of polarization in KNN films.

Fig. 4 displays the capacitance as a function of frequency for Sample A and Sample B at room temperature without applying a magnetic field. The capacitance for both samples is higher at lower frequencies and decreases with the increment of frequency from 100 Hz to 1 MHz, which can be explained by the phenomenon of dipole relaxation wherein at low frequencies the dipoles are able to follow the frequency of the applied field. However, the capacitance of Sample A decreases more rapidly than that of Sample B due to the higher concentration of cation vacancies in Sample A.

Fig. 5 shows the magnetic field dependence of the variation of capacitance at various frequencies at room temperature for Sample A and Sample B. Magnetic field controlled capacitance (MC effect) is defined as $\Delta C/C_0 = [C(H) - C(0)]/C(0)$, where $C(H)$ and $C(0)$ represent the capacitance under field H and without field. The capacitance increases with the applied magnetic field up to 8 kOe. As for Sample A (see Fig. 5(a)), a rather large $\Delta C/C_0$ of 16.73% can be observed at 1 kHz under H = 8 kOe owning to the higher magnetization in Sample A, which results in stronger coupling between magnetization and capacitance through MC effect. In addition, $\Delta C/C_0$ decreases with increasing frequency. However, with regard to Sample B (see Fig. 5(b)), a rather small $\Delta C/C_0$ of 2.28% is obtained at 1 MHz under H = 8 kOe due to the lower concentration of cation vacancies which leads to a weaker MC effect. Additionally, $\Delta C/C_0$ decreases with decreasing frequency, reverse to the tendency for Sample A.

In order to investigate the effect of direct electric field treatment on the magnetization for the KNN film, different electric fields were applied to Sample B for 5 min, respectively. Then the electric field was removed and magnetic measurement was taken one day later. As displayed in Fig. 6(a), the M_s value of the polarized sample increases with the increasing applied electric field. The M_s value of the polarized sample under 10 mV is 0.59 emu/cm^3, which is five times that of the sample absent of electric field treatment. A plot of the measured signal prior to substrate deduction for the 6 mV and 10 mV electric-field treatment is displayed in the inset of Fig. 6(a) to verify that the measured magnetic signal was not from experimental errors or substrate [44,51], as all the measurements were carefully performed and the substrate and probe were both measured to be diamagnetic. Additionally, the KNN film was measured to be insulating with resistance larger than 200 MΩ. The leakage current under the application of 10 mV was 5×10^{-5} mA, equal to 5 μA/cm^2, thus joule heating effect which was proportional to the square of current was negligible in our treatment, in agreement with the result that no obvious difference was observed for Sample B on applying the electric field for 5 min and 10 min. We also measured the magnetization of a sample before and after electrode deposition, no significant difference could be observed, meaning that the influence of metallic contaminants from the electrodes was negligible.

As for the enhancement of M_s, one possibility is that the electrical treatment leads to the change of the KNN film's magnetic anisotropy as in ferromagnetic semiconductors [52,53], resulting in the shift of the magnetization direction from perpendicular to the surface plane to parallel to the surface plane. The higher the

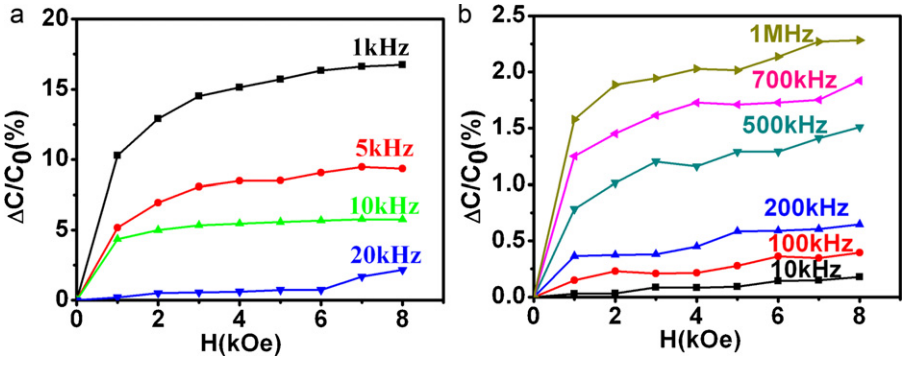

Fig. 5. Magnetic field induced change in capacitance for Sample A (T_s = 700 °C, P_{O_2} = 3 Pa) and Sample B (T_s = 300 °C, P_{O_2} = 3 Pa).

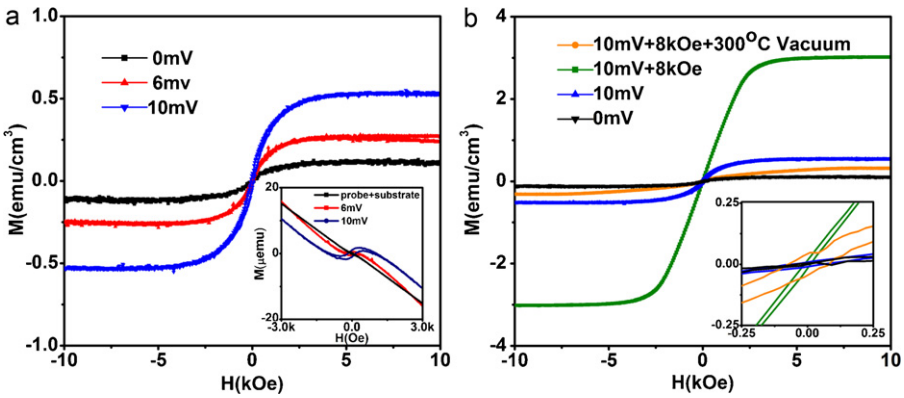

Fig. 6. (a) Field dependence of magnetization for the electric-field treated Sample B (T_s = 300 °C, P_{O_2} = 3 Pa) under different voltages. The inset shows the measured magnetic signal prior to diamagnetic subtraction. (b) Field dependence of magnetization for Sample B after different treatments. The inset represents the field dependence of magnetization in the low field range.

applied electric field, the magnetization projected onto the surface plane would be larger. The behavior is similar to the effect reported by T. Maruyama et al. that a relatively small electric field can cause a large change (40%) in the magnetic anisotropy of a bcc Fe(0 0 1)/MgO(0 0 1) junction [54]. However, the mechanism for ferromagnetic interaction is different: cation vacancies are responsible for the RTFM in our KNN sample, while charge carrier concentration determines the magnetization direction in ferromagnetic semiconductors. More theoretical works are needed to explore how the cation vacancies contribute to the magnetization in KNN.

It has been shown that in multiferroic $CoFe_2O_4/Pb(Mg_{1/3}Nb_{2/3})_{0.7}Ti_{0.3}O_3$ heterostructure, the in-plane magnetization increases under electric field and restores to its initial value after removal of the electric field [55]. However, $(K_{0.5}Na_{0.5})NbO_3$ is both ferroelectric and piezoelectric at room temperature, the application and subsequent removal of an electric field would leave remnant polarization and piezoelectric strain in the sample, which would be coupled to the magnetization of the KNN nanocrystalline film through ME coupling and inverse magnetostrictive effect [56]. The higher the applied electric field, the more remnant polarization and strain would be left in the sample, resulting in the stabilization of the magnetization projected onto the surface plane.

Seem from Fig. 6(b), the M_s value of Sample B after simultaneous treatment of a small electric field (10 mv) and a magnetic field (8 kOe) is 3 emu/cm^3, five times the value of the sample after only electrical treatment. The applied magnetic field was parallel to the surface of the film, namely, perpendicular to the electric field, while the magnetic field for the magnetic measurement was applied parallel to the surface of the film, in other words, the orthometric application of an electric field and magnetic field on the surface of film led to an enormous enhancement of in-plane saturation magnetization. We also found that the M_s value was greatly reduced to 0.38 emu/cm^3 and the coercive force became larger after annealing in vacuum at 300 °C for 20 min (see the inset of Fig. 6(b)). So far as we know, this is a new phenomenon, which has not been reported before, and the origin is still an open problem.

4. Conclusions

In conclusion, we have demonstrated that the room temperature ferromagnetism can be achieved in the pulsed laser deposited $(K_{0.5}Na_{0.5})NbO_3$ nanocrystalline films through the introduction of cation (K, Na) vacancies during deposition at the expense of the deterioration of ferroelectricity. Both magnetic field controlled capacitance and electric field induced enhancement of M_s confirm the coupling between the magnetization and the polarization in the $(K_{0.5}Na_{0.5})NbO_3$ nanocrystalline films at room temperature. The phenomenon that the orthometric application of an electric field and magnetic field on the surface of film and subsequent removal leads to an enormous enhancement of in-plane saturation magnetization in the conventional ferroelectric $(K_{0.5}Na_{0.5})NbO_3$ nanocrystalline films with cation vacancy induced ferromagnetism is intriguing, which can be used for device applications.

Acknowledgements

This work was supported by National Natural Science Foundation of China (Nos. 51072103, 50872074, and 50872069).

References

[1] N.A. Spaldin, M. Fiebig, Science 309 (2005) 391.
[2] W. Eerenstein, N.D. Mathur, J.F. Scott, Nature 422 (2006) 759.
[3] Y. Tokura, Science 312 (2006) 1481.
[4] J.F. Scott, Nat. Mater. 6 (2007) 256.
[5] R. Ramesh, N.A. Spaldin, Nat. Mater. 6 (2007) 21.
[6] X.Q. Zhang, Y. Sui, X.J. Wang, Y. Wang, Z. Wang, J. Alloys Compd. 507 (2010) 157–216.
[7] J.G. Wu, J. Wang, J. Alloys Compd. 507 (2010) L4–L7.
[8] X.D. Qi, W.-C. Chang, J.-C. Kuo, I.-G. Chen, Y.-C. Chen, C.-H. Ko, J.-C.-A. Huang, J. Eur. Ceram. Soc. 30 (2010) 283–287.
[9] F. Azough, R. Freer, M. Thrall, R. Cernik, F. Tuna, D. Colliso, J. Eur. Ceram. Soc. 30 (2010) 727–736.
[10] F. Yan, T.J. Zhu, M.O. Lai, L. Lu, Scripta Mater. 63 (2010) 780–783.
[11] S.K. Pradhan, J. Das, P.P. Rout, V.R. Mohanta, S.K. Das, S. Samantray, D.R. Sahu, J.L. Huang, S. Verma, B.K. Roul, J. Phys. Chem. Solids 71 (2010) 1557–1564.
[12] J. Liu, M.Y. Li, L. Pei, J. Wang, B.F. Yu, X. Wang, X.Z. Zhao, J. Alloys Compd. 493 (2010) 544–548.
[13] S.Y. Chen, L.Y. Wang, H.C. Xuan, Y.X. Zheng, D.H. Wang, J. Wu, Y.W. Du, Z.G. Huang, J. Alloys Compd. 506 (2010) 537–540.
[14] B.-C. Luo, C.-L. Chen, Z. Xu, Q. Xie, Phys. Lett. A 374 (2010) 4265–4268.
[15] M. Venkatesan, C.B. Fitzgerald, J.M.D. Coey, Nature 430 (2004) 630.
[16] N.H. Hong, J. Sakai, N. Poirot, V. Brizé, Phys. Rev. B 73 (2006) 132404.
[17] N.H. Hong, N. Poirot, J. Sakai, Phys. Rev. B 77 (2008) 033205.
[18] A. Sundaresan, R. Bhargavi, N. Rangarajan, U. Siddesh, C.N.R. Rao, Phys. Rev. B 74 (2006) 161306.
[19] J.F. Hu, Z.L. Zhang, M. Zhao, H.W. Qin, M.H. Jiang, Appl. Phys. Lett. 93 (2008) 192503.
[20] J.I. Beltrán, C. Monty, Ll. Balcells, C. Martinez-Boubeta, Solid State Commun. 149 (2009) 1654.
[21] N. Kumar, D. Sanyal, A. Sundaresan, Chem. Phys. Lett. 477 (2009) 360.
[22] J.M.D. Coey, M. Venkatesan, P. Stamenov, C.B. Fitzgerald, L.S. Dorneles, Phys. Rev. B 72 (2005) 024450.
[23] C.D. Pemmaraju, S. Sanvito, Phys. Rev. Lett. 94 (2005) 217205.
[24] C.M. Araujo, M. Kapilashrami, X. Jun, O.D. Jayakumar, S. Nagar, Y. Wu, C. Århammar, B. Johansson, L. Belova, R. Ahuja, G.A. Gehring, K.V. Rao, Appl. Phys. Lett. 96 (2010) 232505.
[25] C. Martínez-Boubeta, J.I. Beltrán, Ll. Balcells, Z. Konstantinović, S. Valencia, D. Schmitz, J. Arbiol, S. Estrade, J. Cornil, B. Martínez, Phys. Rev. B 82 (2010) 024405.
[26] R.V.K. Mangalam, N. Ray, U.V. Waghmare, A. Sundaresan, C.N.R. Rao, Solid State Commun. 149 (2009) 1.

[27] L. Sun, J.F. Hu, F. Gao, X.W. Kong, H.W. Qin, M.H. Jiang, J. Alloys Compd. 502 (2010) 176–179.
[28] J. Rodel, W. Jo, K. Seifert, E.-M. Anton, T. Granzow, D. Damjanovic, J. Am. Ceram. Soc. 92 (2009) 1153–1177.
[29] R.Z. Zuo, D.Y. Lv, J. Fu, Y. Liu, L.T. Li, J. Alloys Compd. 476 (2009) 836–839.
[30] L.K. Su, K.J. Zhu, L. Bai, J.H. Qiu, H.L. Ji, J. Alloys Compd. 493 (2010) 186–191.
[31] T.A. Skidmore, T.P. Comyn, S.J. Milne, J. Am. Ceram. Soc. 93 (2010) 624–626.
[32] M.H. Jiang, X.Y. Liu, G.H. Chen, Scripta Mater. 60 (2009) 909–912.
[33] Q. Zhang, B.P. Zhang, H.T. Li, P.P. Shang, J. Alloys Compd. 490 (2010) 260–263.
[34] Q.Y. Yin, S.G. Yuan, Q. Dong, C.G. Tian, J. Alloys Compd. 491 (2010) 340–343.
[35] X.H. Li, J.L. Zhu, M.S. Wang, J. Alloys Compd. 499 (2010) L1–L4.
[36] J.G. Wu, J. Wang, J. Appl. Phys. 106 (2009) 066101.
[37] H.J. Lee, I.W. Kim, J.S. Kim, C.W. Ahn, B.H. Park, Appl. Phys. Lett. 94 (2009) 092902.
[38] C.R. Cho, A. Grishin, Appl. Phys. Lett. 75 (1999) 268.
[39] J. Miao, X.G. Xu, Y. Jiang, L.X. Cao, B.R. Zhao, Appl. Phys. Lett. 95 (2009) 132905.
[40] C.R. Cho, Mater. Lett. 57 (2002) 781–783.
[41] X. Yan, W. Ren, X.Q. Wu, P. Shi, X. Yao, J. Alloys Compd. 508 (2010) 129–132.
[42] F.P. Lai, J.F. Li, J. Sol–Gel Sci. Technol. 42 (2007) 287–292.
[43] P.C. Goh, K. Yao, Z. Chen, Appl. Phys. Lett. 97 (2010) 102901.
[44] M.A. Garcia, E.F. Pinel, J. de la Venta, A. Quesada, V. Bouzas, J.F. Fernández, J.J. Romero, M.S. Martín González, J.L. Costa-Krämer, J. Appl. Phys. 105 (2009) 013925.
[45] C. Zaldo, D.S. Gill, R.W. Eason, J. Mendiola, P.J. Chandler, Appl. Phys. Lett. 65 (1994) 502–504.
[46] K.J. Choi, M. Biegals, Y.L. Li, A. Sharan, J. Schubert, R. Uecker, P. Reiche, Y.B. Chen, X.Q. Pan, V. Gopalan, L.-Q. Chen, D.G. Schlom, C.B. Eom, Science 306 (2004) 1005.
[47] L. Qiao, X.F. Bi, Thin Solid Films 517 (2009) 3784.
[48] J.F. Scott, J. Phys.: Condens. Matter. 20 (2008) 021001.
[49] N.M. Hagh, E. Ashbahian, A. Safari, IEEE Trans. Ultrason. Ferroelectr. Freq. Control 55 (2008) 214–224.
[50] L.J. Wang, S.M. Feng, J.L. Zhu, R.C. Yu, C.Q. Jin, W. Yu, X.H. Wang, L.T. Li, Appl. Phys. Lett. 91 (2007) 172502.
[51] M. Khalid, A. Setzer, M. Ziese, P. Esquinazi, D. Spemann, A. Pöppl, E. Goering, Phys. Rev. B 81 (2010) 214414.
[52] D. Chiba, M. Yamanouchi, F. Matsukura, H. Ohno, Science 301 (2003) 943.
[53] D. Chiba, M. Sawicki, Y. Nishitani, Y. Nakatani, F. Matsukura, H. Ohno, Nature 455 (2008) 515.
[54] T. Maruyama, Y. Shiota, T. Nozaki, K. Ohta, N. Toda, M. Mizuguchi, A.A. Tulapurkar, T. Shinjo, M. Shiraishi, S. Mizukami, Y. Ando, Y. Suzuki, Nat. Nanotechnol. 4 (2009) 158.
[55] B.D. Cullity (Ed.), Introduction to Magnteic Materials, Addison-Wesly, Reading, 1972, chapter 8.
[56] J.J. Yang, Y.G. Zhao, H.F. Tian, L.B. Luo, H.Y. Zhang, Y.J. He, H.S. Luo, Appl. Phys. Lett. 94 (2009) 212504.